



Deposited amorphous silicon-on-insulator technology for nano-photonic integrated circuits



Shankar Kumar Selvaraja^{a,*}, Marc Schaeckers^a, Wim Bogaerts^b, Dries Van Thourhout^b

^a IMEC, Kapeldreef 75, 3001 Leuven, Belgium

^b Ghent University - IMEC, Department of Information Technology, Sint-Pietersnieuwstraat 41, 9000 Gent, Belgium

ARTICLE INFO

Article history:

Received 4 September 2013

Received in revised form

10 October 2013

Accepted 11 October 2013

Available online 22 October 2013

Keywords:

Nano-photonics

Waveguides

Amorphous silicon

Optical interconnects

Back-end integration

PECVD

ABSTRACT

Low-loss deposited amorphous silicon (α -Si:H) layers for nano-photonic integrated circuit have been prepared using complementary-metal-oxide-semiconductor (CMOS) compatible technology. Waveguide loss as low as 3.45 dB/cm is reported for films deposited at a low temperature (300 °C) using plasma enhanced chemical vapour deposition process. The influence of the deposition parameters such as gas dilution, plasma power and pressure on the quality of the deposited material is thoroughly characterized using Fourier transform infrared spectroscopy (FTIR), spectroscopic ellipsometry, X-ray diffraction and atomic force microscopy. We show that the optical quality of the deposited film can be directly assessed from distinct frequency bands (2090, 2000 and 840 cm^{-1}) using FTIR, without the need for further waveguide loss measurements.

© 2013 Elsevier B.V. All rights reserved.

1. Introduction

Silicon photonics is maturing as an integrated photonics technology platform suitable for various applications. One of the main driving forces behind this development is integration with complementary-metal-oxide-semiconductor (CMOS) technology for next generation high performance computing and data communication. The high-refractive index contrast of silicon with respect to its cladding layers (SiO_2 or air) helps to increase the device density by up to 6 orders of magnitude from traditional silica based photonic circuits. However, further scaling down is limited by the wavelength of light. In order to increase the device density further vertical integration of photonic circuits should be exploited.

Although silicon photonics has made tremendous progress, it has mostly relied on crystalline silicon-on-insulator technology. In spite of the superior material quality, this seriously limits innovation and integration options. It does, for example, not allow for multilayer photonic circuits and also limits the options for integrating electronic and photonic circuits. Various options have been proposed for both these applications, including free space optics but no general consensus has been reached yet. The two main integration routes explored are bonding [1,2] and layer stacking approaches (back-end) [3,4]. Although such 3D integration technologies are widely explored

for electronic–photonics integration, a simple CMOS back-end compatible layered approach would be suitable for most applications, including multilayer photonic integrated circuits, and possibly more cost effective.

To realize a layered integration scheme, the main requirement is the availability of a low-loss core material. Over the last few years, the propagation loss of deposited silicon has been brought down considerably, nearly matching that of crystalline silicon. This has been achieved by exploring different deposition techniques. Various groups showed that plasma enhanced chemical vapour deposition (PECVD) is the most suitable technique to achieve low-loss deposited (amorphous) silicon [5–9,11]. The main reason is the ability to deposit layers with a low number of defects. Furthermore, it is an attractive technique for electronic–photonics back-end integration since the deposition can be done at low temperatures (< 400 °C). Using this technique propagation losses of 2 and 3.45 dB/cm were achieved for respectively low and high contrast waveguide configurations [8,13] and modulators using thermo-optic [14,12], all-optical [7,15] and electro-optic [16] effects within these layers were demonstrated.

Understanding the material properties is the key for preparing high quality deposited amorphous silicon. Despite improvements over the past years, unfortunately, there is no comprehensive material study available investigating deposited silicon optimized for integrated photonics. As low propagation loss is put forward as the main requirement, unless the material properties are thoroughly studied, it will be impossible to improve the layer quality further. In this paper,

* Corresponding author. Tel.: +32 496157736.

E-mail address: selva.shankar@gmail.com (S. Kumar Selvaraja).

Table 1
Comparison of different deposition techniques for Si deposition.

Technique	Temperature	Material phase	Loss mechanism
LPCVD	High	α , Poly	Scattering, absorption
Epitaxy	High	Crystalline	Absorption
PECVD	Low	α , Poly	Scattering, absorption
Sputtering	Low	α	Absorption
E-gun evaporation	Low	α	Absorption

α , amorphous; Poly, polycrystalline including nano- and microcrystalline.

we relate the deposition parameters to the material properties of the deposited layers and explain how the latter then influence the propagation loss in the 1550 nm telecom wavelength band.

2. Deposited amorphous silicon

Silicon (Si) can be deposited using different techniques and conditions. Table 1 summarizes different techniques to choose from. The ability to control scattering and absorption loss determines the suitability of a technique for obtaining high quality films. These losses are caused by defects in the material. We can discern two categories of defects. On one hand, hard defects, which cannot be removed from the film; on the other hand, soft defects, which can be reduced after deposition. Material defects such as voids, grain boundaries, dangling bonds and interface defects can be classified as hard defects, while stress and surface roughness are classified as soft defects. The presence of voids and grain boundaries causes scattering of light, while the presence of dangling bonds causes absorption of light. Thus, to achieve low propagation loss, the material should not have grains (i.e. be amorphous or mono-crystalline), should be free of voids and should have a low number of Si dangling bonds.

As previously mentioned (Section 1) the PECVD technique is the most viable technique for low-loss α -Si deposition. One of the main reasons is that the absorption in the electronic bandgap due to dangling bonds can be resolved during deposition by incorporating hydrogen (H) in the Si network resulting in hydrogenated amorphous silicon (α -Si:H). The scattering loss can then be reduced by tuning the deposition conditions to deposit non-crystalline and void free amorphous films. Though hydrogen plays an important role in reducing the propagation loss [17], there is an optimum level above which it plays a negative role.

3. Plasma enhanced chemical vapour deposition

Plasma enhanced chemical vapour deposition is a popular method for thin film deposition in microelectronics. Although mainly used for dielectric deposition it is also used for semiconductor and metal deposition. Fig. 1 illustrates a simple PECVD system with the essential components. By applying a radio frequency voltage across the electrodes, and in the presence of sufficient gas molecules, a plasma is created. The wafer (or substrate) is brought in contact with one of the electrodes to attract the radicals to the surface resulting in film formation. The film deposition and its properties can be tuned by the deposition process parameters: substrate temperature, plasma power, pressure, gas flow and spacing between the electrodes.

3.1. Growth process overview

α -Si:H thin films for photonics are commonly prepared using monosilane (SiH_4) as precursor gas with or without dilution gases such as H_2 , He, Ar, and Xe. In the plasma, the precursor gas is dissociated into different reactive species, including silyl (SiH_3), silylene (SiH_2), silylidine (SiH), etc., depending on the energy state.

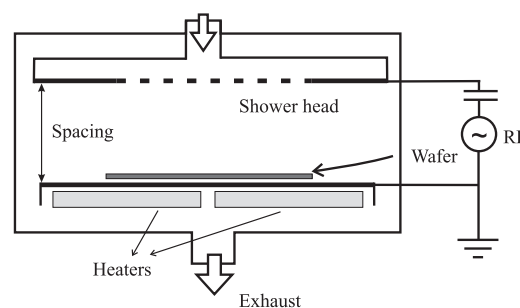


Fig. 1. Schematic of a simple plasma enhanced chemical vapour deposition system.

Table 2
Experimental condition.

Parameter	Range	Nominal setting
RF power (W)	100–300	180
Spacing	500 mils (12.25 mm)	500 mils
Pressure (Torr)	1.5–5	2.6
Temperature ($^{\circ}\text{C}$)	300	300
Silane (SiH_4) flow (sccm)	100–300	100
Helium (He) flow (sccm)	0–2500	900

These excited species react among themselves and with the feed gas to form a steady state condition to sustain the plasma.

It has been shown by Matsuda et al. [18,19] that SiH_3 is one of the dominant species in the plasma and also one of the major contributors for the film growth. By adsorbing these species on the surface of the wafer a solid film can be formed from the gaseous species. Initially, the wafer surface is covered with -H . When the Si containing radicals arrive onto the H-rich surface it reacts with H, which is then released from the surface (Eqs. (1) and (2)), resulting in a dangling bond. This dangling bond serves as a growth point for further film formation. However, not all of these dangling bonds are further used, hence leaving residual defects. Thus, it is not possible to prepare films without defects (i.e. dangling bonds):



3.2. Experimental conditions

α -Si:H is deposited in a 200 mm industrial PECVD deposition tool (Applied Materials Centura 5200). The deposition chamber is a part of a deposition cluster with load-locks. The plasma source consists of two aluminium electrodes separated by a gap set to 12.25 mm. The upper electrode is connected to a radio frequency power supply operating at 13.56 MHz, while the bottom electrode is grounded. SiH_4 and helium (He) are used for film deposition. As mentioned earlier there are a number of parameters that can be tuned to control the film growth. We kept the substrate temperature and the distance between the electrodes (spacing) constant, while the feed gas ratio, pressure, and power were tuned. Table 2 summarizes the experimental conditions of the deposition process used in our experiments.

4. Material characterization

The material properties of the deposited α -Si:H are characterized using the following techniques:

1. Spectroscopic ellipsometry/KLA-Tencor ASET-F5 – thickness and refractive index measurements.

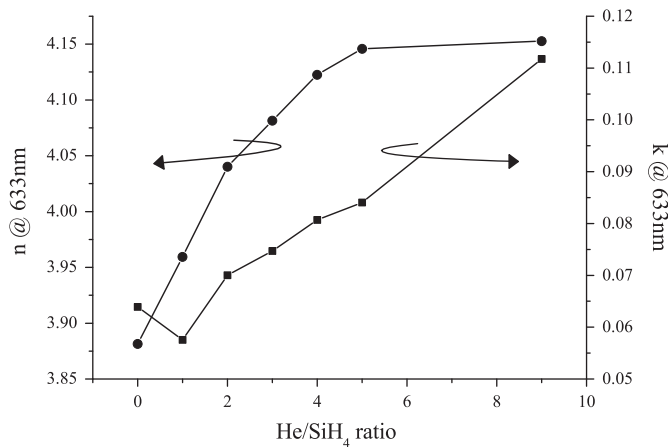


Fig. 2. Influence of dilution of SiH₄ on the refractive index ($n&k$) at 633 nm.

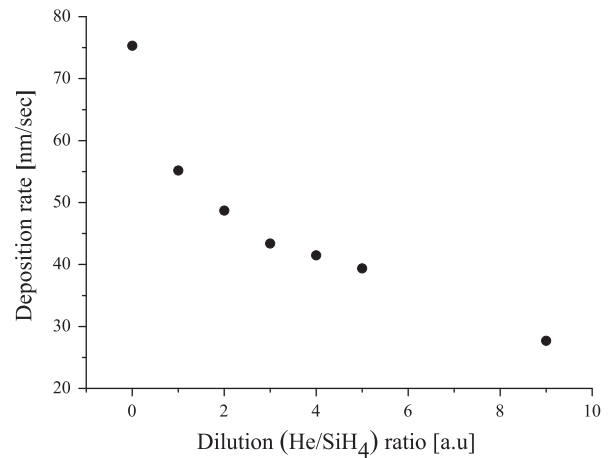


Fig. 3. Influence of dilution of SiH₄ on the Deposition rate of α -Si:H.

- Fourier transform infrared spectroscopy (FTIR)/Bio-rad FTS 40 – film composition (different Si–H bond configurations).
- X-ray diffraction/Bede Metrix™–L – crystal structure characterization.
- Laser scanning /Eichhorn Hausman Stress Meter MX203 – stress and wafer bow characterization.
- Atomic force microscopy/Veeco Nanoscope IV Dimension 3100 – surface morphology characterization.
- Optical transmission (cut-back method) – waveguide propagation loss characterization.

4.1. Deposition rate and refractive index

The film thickness and the refractive index of the deposited material were characterized using spectroscopic ellipsometry. Figs. 2 and 3 illustrate the effect of dilution of the precursor (SiH₄) on the refractive index and deposition rate of the deposited films respectively. The refractive index of the film increases with an increase in the dilution, which induces an increase in film density, while the deposition rate decreases. We also observe that the refractive index decreases with an increase in power (Fig. 4).

The change in the film density can be related to the deposition rate. The growth process itself is a complex sequence of random events on the wafer surface. However, a simple but realistic explanation can be considered. The deposition rate increases with an increase in the radical density in the plasma. This can happen either at higher plasma powers or at lower dilution. During the growth process, the radicals from the plasma arrive on the wafer surface at a certain rate called radical arrival rate R_a , which is determined by the deposition condition. Upon arrival on the surface, these radicals diffuse to identify a reactive growth site, the distance they travel on the surface is called diffusion length and the rate at which they react is called the surface reaction rate (R_{sr}). If R_{sr} is higher than R_a , the radical gets sufficient time to find a growth centre resulting in a dense film; on the other hand, if $R_{sr} < R_a$ a less dense film is formed.

4.2. Film composition

The composition of the deposited film is studied through the FTIR absorbance spectrum between 400 and 4000 cm⁻¹. The background corrected spectrum is studied for the Si–H bond configurations, as they are an important constituent of the film. The characteristic vibration modes of different Si–H bonds occur at distinct frequencies, which are summarized in Table 3. Although H

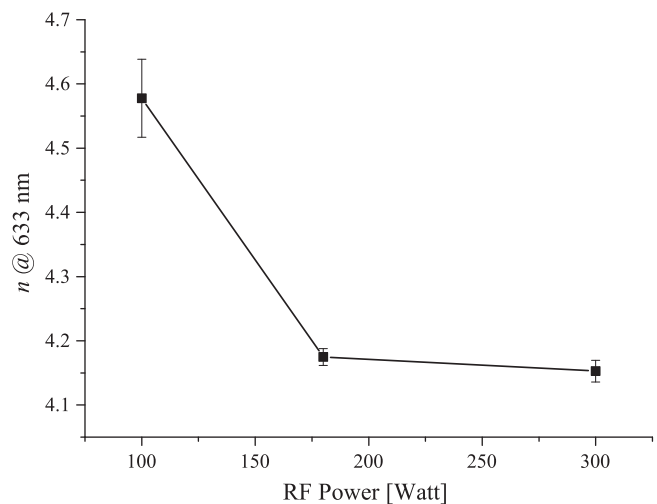


Fig. 4. Influence of plasma power on the refractive index of α -Si:H.

Table 3

Infrared absorption of various Si–H_n vibration modes.

Bond configuration	Peak frequencies (cm ⁻¹)	Ref
Si–H wagging	640	[20,21]
Si–H ₂ rocking	620	[20]
Si–H ₃ symmetric bending	840	[20,22]
Si–H ₃ asymmetric	890	[20,22]
Si–H ₂ symmetric bending	890	[20,22]
Si–H stretching	2000	[20]
Si–H ₂ asymmetric stretching	2090	[20]
Si–H ₃ symmetric stretching	2090	[20]

is a vital element for preparing low-loss α -Si films higher concentrations lead to undesirable cluster formation, which can result in void formation. These clusters can be easily identified from the IR frequency peaks in the spectrum as presented in Table 3.

4.2.1. Effect of dilution

Figs. 5 and 6 depict the absorbance spectra at 2000 and 640 cm⁻¹ for samples with different dilution. In Fig. 5 it can be clearly seen that the peak shifts from 2090 cm⁻¹ (polyhydride) to 2000 cm⁻¹ (monohydride). This is a clear indication that the total

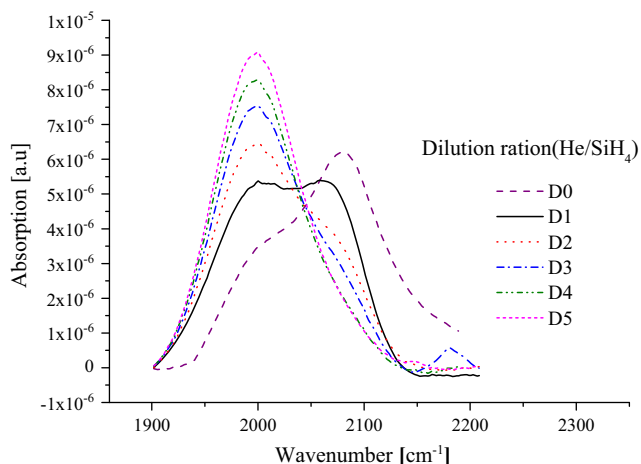


Fig. 5. Infrared absorption due to $\text{SiH}_{x=1,2,3}$ at 2000 and 2090 cm^{-1} , at different precursor dilutions. In legend Dx, x represent dilution ratio of He/SiH_4 .

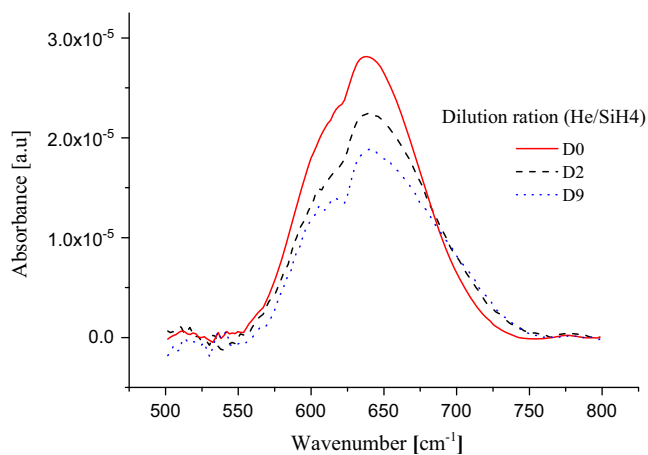


Fig. 6. Infrared absorption due to SiH at 640 cm^{-1} , at different precursor dilutions. In legend Dx, x represent dilution ratio of He/SiH_4 .

amount of H incorporated in the film decreases with an increase in dilution. Furthermore it is evident from the reduction in the 640 cm^{-1} Si-H peak with increasing dilution that the total H incorporation in the film is reduced with increasing dilution (Fig. 6). Excessive hydrogen in the film creates voids, which is called microstructure (R). The latter is often quantified by the ratio of mono- and polyhydrides absorbance peaks:

$$R = \frac{\int I_{2090}}{\int I_{2000} + \int I_{2090}}, \quad (3)$$

where I_{2000} and I_{2090} are the integrated intensities of the peaks at 2000 and 2090 cm^{-1} respectively. Fig. 7 shows the microstructure R obtained from the spectrum, which clearly indicates the reduction in the voids with increasing dilution. The microstructure is an indication of the film density and can be correlated with the refractive index of the film. We indeed observe an excellent agreement between these two quantities when comparing Figs. 2 and 7.

4.2.2. Effect of pressure

The effect of the pressure on the deposited film was studied while keeping other plasma parameters constant: precursor dilution at $\text{He}/\text{SiH}_4=9$, spacing at $500 \text{ mils}/12.25 \text{ mm}$, power at 100 W and temperature at $300 \text{ }^\circ\text{C}$. The pressure was varied from 1.5 to

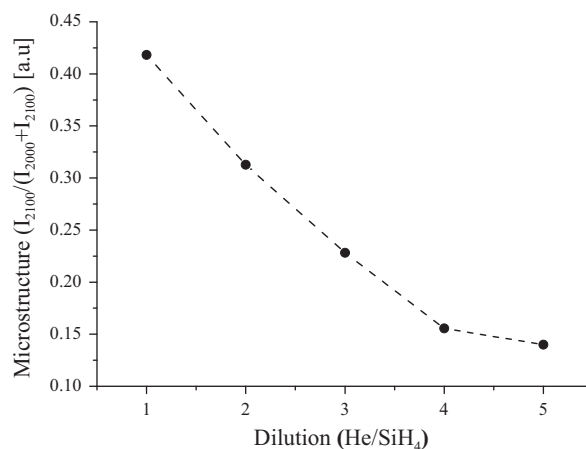


Fig. 7. Microstructure evaluation as a function of precursor dilution.

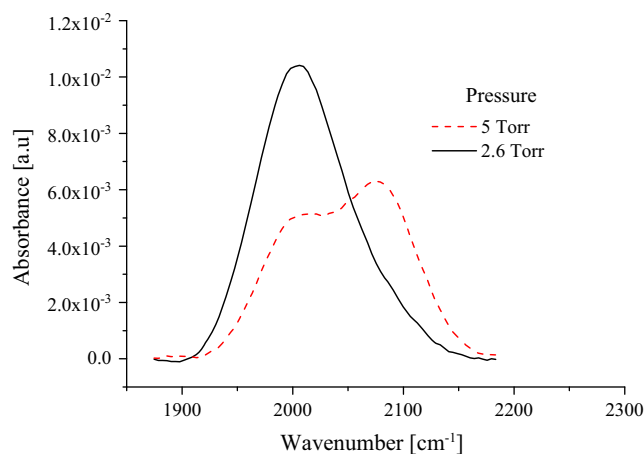


Fig. 8. Influence of pressure on the infrared absorption due to mono- and polyhydrides of SiH_x at 2000 and 2090 cm^{-1} respectively.

5 Torr . At the lowest pressure (1.5 Torr) the plasma failed to ignite, hence no deposition was possible at this pressure.

Fig. 8 depicts the absorbance spectrum in the $2000\text{--}2090 \text{ cm}^{-1}$ band. At higher pressure the absorbance at 2090 cm^{-1} indicates formation of clustered SiH and $\text{SiH}_{x=2,3}$. However this peak disappears at low pressure, which can be attributed to a decrease in the radical density in the plasma at lower pressure. This can be explained as follows: at a constant gas flow, when the pressure is increased the mean free path of the gas molecules is reduced. This leads to a chain reaction between the precursor (SiH_4) and dissociated radicals (e.g. SiH_2) forming $(\text{Si-H}_{2,3})_n$ like networks [23]. This is verified from the absorption peak around 840 and 890 cm^{-1} (Fig. 9), which corresponds to clustered Si-H_3 and Si-H_2 respectively. The peak at 840 and 890 cm^{-1} diminishes when the pressure is decreased, which clearly indicates that at lower pressure the $(\text{Si-H}_{2,3})_n$ chain formation is arrested, resulting in the formation of void free and dense film.

4.2.3. Effect of power

The power applied to create the plasma is an important deposition parameter, which facilitates dissociation of the precursor gas. To study the effect of applied power on the film composition the applied power is changed between 100 and 300 W , while the other parameters were kept constant at their nominal value as indicated in Table 2.

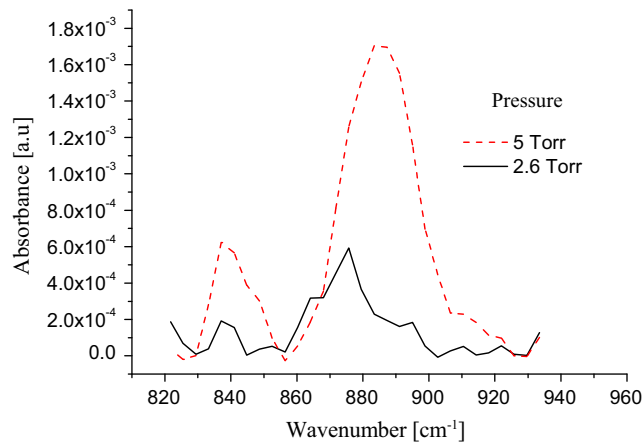


Fig. 9. Influence of pressure on the infrared absorption due to SiH₂ chains at 840 and 890 cm⁻¹.

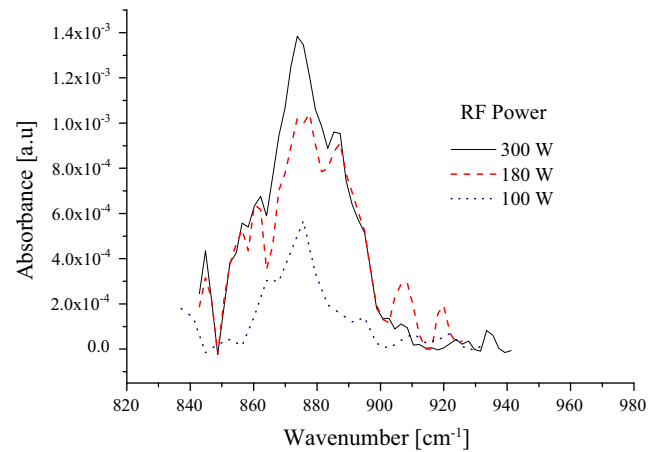


Fig. 11. Influence of plasma power on the infrared absorption due to clustered Si-H₃ and Si-H₂ at 840 and 890 cm⁻¹ respectively.

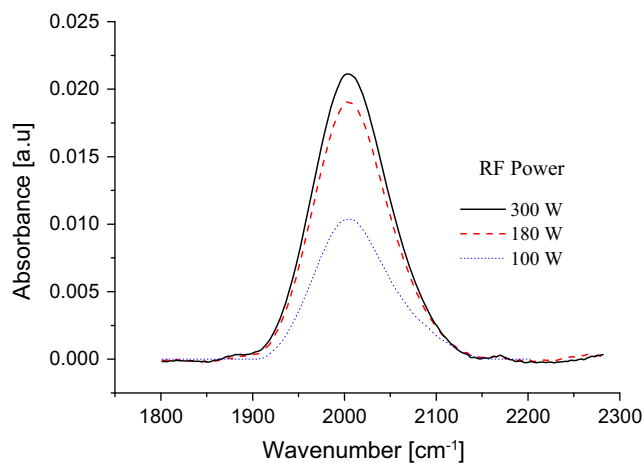


Fig. 10. Influence of plasma power on the infrared absorption due to mono- and polyhybrid of SiH_x at 2000 and 2090 cm⁻¹ respectively.

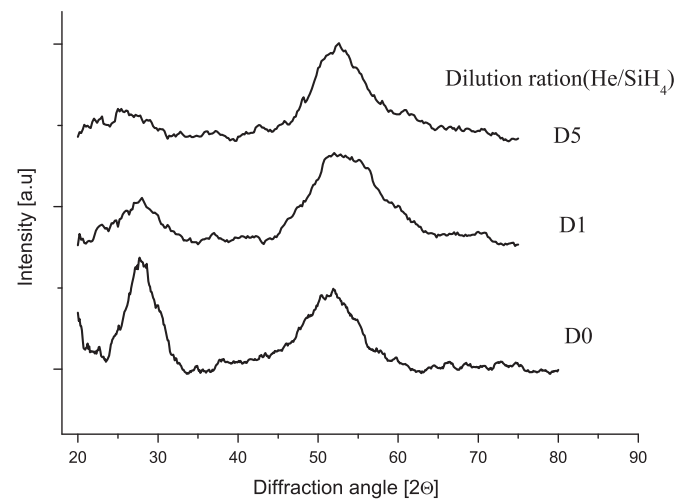


Fig. 12. X-ray diffraction spectrum of α -Si:H films deposited with different silane dilutions. In legend Dx, x represent dilution ratio of He/SiH₄.

We observe an increase in the Si-H monohydride peak (2000 cm⁻¹) with an increase in applied power (Fig. 10), while no polyhybrid peak (2090 cm⁻¹) was observed. However, the clustered Si-H₂ peak at 890 cm⁻¹ appears at higher power and diminishes when the power is reduced (Fig. 11). Due to the existence of a higher radical density at high plasma power the chain reaction leads to (SiH₂)_n formation, which is reduced at lower plasma power. From the literature, we have found that better quality α -Si:H is often achieved at low plasma power [5,9]. We believe that the reduction in (SiH₂)_n is one of the reasons for this.

4.3. Crystallography

The crystalline nature of the deposited film was studied using glancing angle (1°) X-ray diffraction (XRD). The measurements were compared with the ones obtained from SE and FTIR presented in Sections 4.1 and 4.2 respectively.

Fig. 12 shows the crystallinity of films deposited with different silane dilutions. Two peaks can be distinguished in the spectrum. The broad peak around $\approx 52^\circ$ could be either from thermal vibration of the substrate Si lattice or $\langle 311 \rangle$ lattice [10]. The peak at 28° corresponds to the Si $\langle 111 \rangle$ crystal in the deposited film. This peak smears out and disappears with an increase of the precursor dilution, which indicates that the film evolves from a microcrystalline phase (at low dilution) to an amorphous phase (at higher dilution). The

crystallinity of the film is also a good indication of the film density: we observe an excellent agreement between SE (Fig. 2) and XRD characterization. As discussed earlier in Section 4.1 with increasing dilution the film density increases due to sufficient incubation time on the wafer surface. During the network formation, the radicals are tightly bound in a random fashion creating a highly dense (also evident from stress) amorphous film. However, at lower dilutions due to less incubation time, the radical cannot form a tighter bond but rather as stacking of the species. Another reason for microstructure/crystalline formation at low dilution is insufficient dissociation of the precursor yielding polyhydrides.

4.4. Film stress

The two main reasons for having stress in a thin film are molecular interactions and differential thermal expansion coefficients (TEC). The stress (σ) induces wafer bow and therefore, can be determined from the wafer curvature. The stress induced by a given layer is calculated from measuring the wafer radius before and after the deposition. This also allows to determine if the stress is either tensile or compressive. Eq. (4) relates stress and the wafer parameters:

$$\sigma = \frac{1}{6} \frac{Y}{1-\nu} \frac{t_s^2}{t_f} \left[\frac{1}{R_f} - \frac{1}{R_s} \right], \quad (4)$$

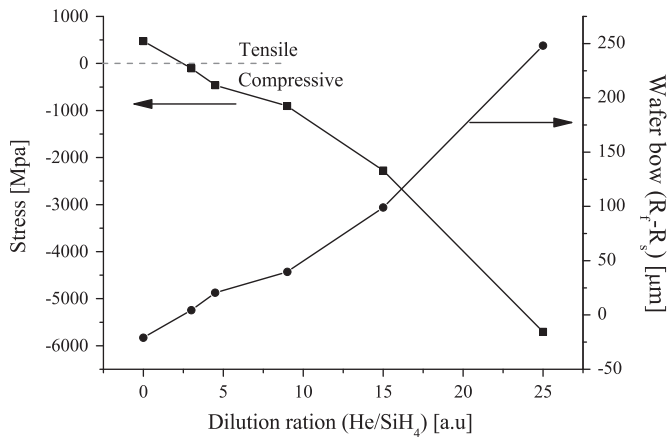


Fig. 13. The effect of dilution on the stress and wafer bow of ≈ 220 nm α -Si:H film. Wafer bow = $R_s - R_f$, where R_s and R_f are the wafer radius before and after deposition respectively.

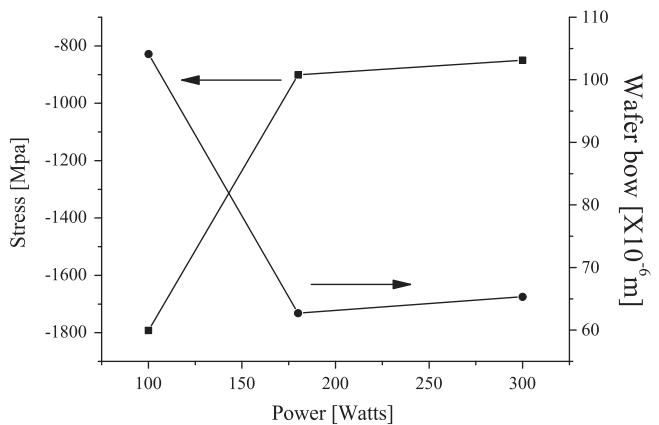


Fig. 14. The effect of plasma power (with other parameters set at nominal condition) on the stress and wafer bow of ≈ 220 nm α -Si:H film. Wafer bow = $R_s - R_f$, where R_s and R_f are the wafer radius before and after deposition respectively.

where t_s is the thickness of the silicon substrate, t_f is the thickness of the deposited film, R_s and R_f are the wafer radius before and after deposition respectively, ν is Poisson's ratio of the wafer and Y is Young's modulus of the substrate.

Figs. 13 and 14 show the effect of dilution and plasma power on the stress in the deposited α -Si:H film. We observe that the stress is mostly compressive, and it increases with an increase in dilution and on the contrary, decreases with an increase in the plasma power. The stress changes from tensile to compressive when the feed gas dilution is increased from 0 to 25. This transition can be explained from the changing diffusion length of the radicals on the surface. As mentioned earlier (in Section 4.1) at higher radical arrival rate (R_{ar}), the diffusion length is restricted, and this results in a columnar structure. Due to inter-molecular attraction between the Si atoms in the columns, neighbouring columns induce a tensile stress. On the other hand, at higher dilution (or lower R_{ar}) the densely packed Si atoms repel each other resulting in a compressive stress (Fig. 14).

From FTIR and XRD characterization, we observe that higher dilution and lower power yield films with low microstructure, which is important to achieve low-loss waveguides. Although stress in itself does not affect the propagation loss, the wafer bow (Figs. 13 and 14) of the films deposited at low power and high dilution is unacceptable for further processing, e.g. during the lithography process, the focus over a wafer with bow will vary resulting in a large variation in the linewidth [24]. For larger bow,

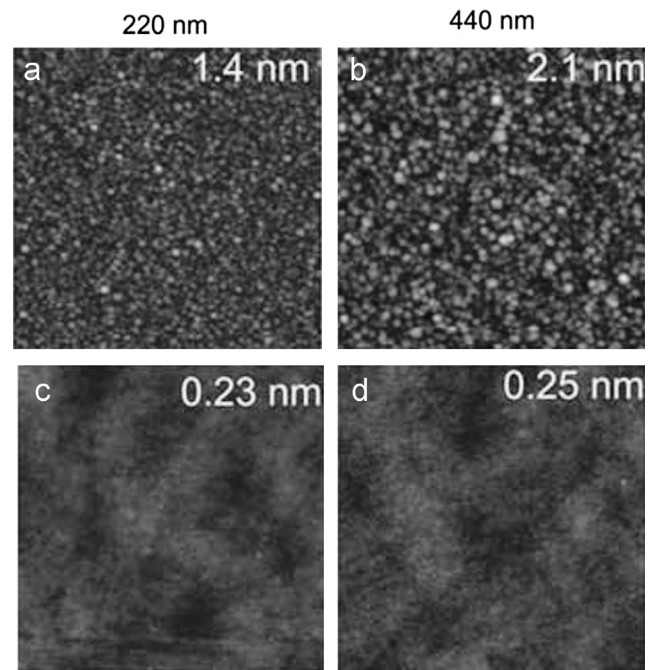


Fig. 15. Surface roughness before (a,b) and after (c,d) polishing of 220 and 440 nm α -Si:H.

the substrate holder used in the lithography tool will reject the wafer. Hence we had to limit our deposition parameters feed gas dilution and power to ≤ 9 and ≥ 180 W respectively.

4.5. Surface morphology

The surface roughness of the film deposited with the optimized deposition condition (180 W, 2.6 Torr, precursor dilution 9) was characterized using atomic force microscopy (AFM). The surface roughness of deposited films is often influenced by substrate roughness, and therefore, we prepared all the films on a polished oxide surface with a surface roughness of 0.1 nm rms. We found that the surface roughness of α -Si:H films increases with an increase in the thickness of the film. A roughness of 1.4 and 2.1 nm was measured for a film thickness of 220 and 440 nm respectively (Fig. 15). As the surface roughness of the film can cause scattering of light eventually resulting in propagation loss, we have used chemical mechanical polishing (CMP) to smoothen the surface. After polishing the surface roughness of the films was 0.23 nm and 0.25 nm for 220 nm and 440 nm thick films respectively. During CMP ≈ 40 nm of material is consumed, which should be taken into account during the initial deposition process.

5. Optical loss measurements

The optical propagation loss of the deposited α -Si:H films in the telecommunication wavelength range 1500–1600 nm was studied through the definition and characterization of photonic wire waveguides. The propagation loss of a photonic wire waveguide is mainly caused by three phenomena: scattering of light from the sidewalls of the photonic wire, scattering of light inside the core due to voids/microstructures and absorption in the core. The propagation loss measurement gives the combined effect of these three loss factors. We studied the effect of the precursor gas dilution and the plasma power on the propagation loss of qTE mode in the photonic wires.

Table 4

Propagation loss of α -Si:H photonic wires for various precursor gas dilution and pressure, while other parameters were kept constant (wafer temperature=300 °C, Pressure=2.6 Torr, spacing=500 mils/12.25 mm).

Material	Dilution ratio (He/SiH ₄)	Power (W)	Wire loss (dB/cm)
α -Si:H	9	100	NA
α -Si:H	9	180	3.46 ± 0.04
α -Si:H	9	300	3.7 ± 0.08
α -Si:H	5	180	4.25 ± 0.04
α -Si:H	3	180	4.94 ± 0.04
α -Si:H	0	180	very high
Crystalline Si	–	–	2.8 ± 0.09

The photonic wires were fabricated in as-deposited α -Si:H of 220 nm on top of 1950 nm of surface polished high-density plasma oxide. Photonic wire patterns with varying length (0.6–6 cm) were defined using 193 nm optical lithography and dry etching. The linewidth of the photonic wires was kept at \approx 450 nm. The details of the fabrication process can be found elsewhere [24]. To compare different materials, we used the same fabrication process for all wafers, thereby keeping the effect of the sidewall roughness fixed. As crystalline silicon is a well known low loss material, we have also fabricated photonic wires in a crystalline Si wafer for comparison.

To characterize the propagation loss of the different materials, light from a broad-band light source is coupled into the waveguide and the output is measured using a spectrum analyzer. We use TE grating fiber couplers [25] to couple the light in and out of the photonic wires. Table 4 summarizes the effect of precursor gas dilution and plasma power on the propagation loss. The propagation loss does not change appreciably with decreasing plasma power (180–300 W). As mentioned earlier we were unable to pattern the film deposited at 100 W due to wafer bow, which restricted us to operation above 100 W. On the other hand, higher dilution clearly shows a considerable improvement in the propagation loss, from immeasurably high loss to 3.46 dB/cm. To our knowledge this is the lowest propagation loss reported for photonic wires of this dimension (450 × 220 nm) fabricated in α -Si:H.

6. Conclusion

A comprehensive material property study has been performed on amorphous silicon α -Si:H, deposited using a PECVD process. We investigated and correlated the effects of different process parameters including the dilution ratio, the plasma power and the chamber pressure on the material properties. In particular, we have found that at a low plasma power, low pressure and higher dilution the film properties are ideal for depositing low-loss α -Si:

H. These parameters can vary slightly depending on the type and size of the deposition chamber. At the optimum deposition condition propagation loss as low as 3.46 dB/cm has been achieved for photonic wire waveguides of 450 nm wide and 220 nm thick.

Acknowledgement

The authors would like to thank G. Bryce, P. Dumon and S. Vanhaelemeersch for their fruitful discussion. This work was partly supported by the European Union through the ICT WADI-MOS project.

References

- [1] J.A. Kash, in: Proceedings of Photonics in Switching, 2007, pp. 55–56.
- [2] B. Liu, A. Shakouri, P. Abraham, J.E. Bowers, Electron. Lett. 35 (1999) 1552.
- [3] I. O'Connor, F. Gaffiot, Ultra Low-Power Electronics and Design, Kluwer, 2004.
- [4] J.M. Fedeli, S. Jeannot, V. Jousseume, L. Di Cioccio, M. Kostrzewa, R. Orobtcouk, P. Maury, M. Zussy, Proc. SPIE 5956 (2005) 595607.
- [5] A.M. Agarwal, M.A. Beals, J. Michel, L.C. Kimerling, D.K. Sparacin, R. Sun, in: Proceedings of Group IV Photonics, 2006, Ottawa, pp. 255–257.
- [6] R. Sun, K. McComber, J. Cheng, D.K. Sparacin, M. Beals, J. Michel, L.C. Kimerling, Appl. Phys. Lett. 94 (2009) 141108.
- [7] K.-Y. Wang, K.G. Petrillo, M.A. Foster, A.C. Foster, Opt. Express 20 (2012) 24600.
- [8] A. Harke, M. Krause, J. Mueller, Electron. Lett. 41 (2005) 1377.
- [9] D. Dai, L. Liu, L. Wosinski, S.A. He, S. He, Electron. Lett. 42 (2006) 400.
- [10] L.K. Bekessy, N.A. Raftery, S. Russell, JCPDS-International Centre for Diffraction Data 2007, pp. 177–181.
- [11] G. Cocorullo, F.G. Della Corte, R. De Rosa, I. Rendina, A. Rubino, E. Terzi, IEEE J. Sel. Top. Quantum Electron. 4 (1998) 997.
- [12] S.K. Selvaraja, W. Bogaerts, D. VanThourhout, M. Schaeckers, D. Van Thourhout, Appl. Phys. Lett. 97 (2010) 071120.
- [13] S.K. Selvaraja, E. Slecckx, M. Schaeckers, W. Bogaerts, D. Van Thourhout, P. Dumon, R. Baets, Opt. Commun. 282 (2009) 1767.
- [14] G. Cocorullo, F.G. Della Corte, R. De Rosa, I. Rendina, A. Rubino, E. Terzini, J. Non-Cryst. Solids 266 (2000) 1247.
- [15] Dong-Jin Won, Mariola O. Ramirez, Hoonsoo Kang, Venkatraman Gopalan, Neil F. Baril, Jacob Calkins, John V. Badding, Pier J.A. Sazio, J. Appl. Phys. 91 (2007) 161112.
- [16] K. Preston, S. Manipatrani, A. Gondarenko, C.B. Poitras, M. Lipson, Opt. Express 17 (2009) 5118.
- [17] Shankar Kumar Selvaraja, Wim Bogaerts, Dries Van Thourhout, Roel Baets, March Schaeckers, Erik Slecckx, in: Proceedings of Symposium IEEE LEOS Benelux chapter, 2007, Eindhoven, pp. 15–19.
- [18] A. Matsuda, Plasma Phys. Control. Fusion 39 (1997) 431.
- [19] A. Matsuda, K. Tanaka, J. Appl. Phys. 60 (1986) 2351.
- [20] M.H. Brodsky, M. Cardona, J.J. Cuomo, Phys. Rev. B Condens. Matter 16 (1977) 3556.
- [21] A.A. Langford, M.L. Fleet, B.P. Nelson, W.A. Lanford, N. Maley, Phys. Rev. B Condens. Matter 45 (1992) 13367.
- [22] G. Lucovsky, R.J. Nemanich, J.C. Knights, Phys. Rev. B Condens. Matter 19 (1979) 2064.
- [23] M. Kawase, T. Masuda, M. Nagashima, T. Maki, Y. Miyamoto, K. Hashimoto, Jpn. J. Appl. Phys. Part 1 33 (1994) 3830.
- [24] S.K. Selvaraja, P. Jaenen, W. Bogaerts, D. Van Thourhout, P. Dumon, R.G. Baets, J. Lightwave Technol. 27 (2009) 4076.
- [25] D. Taillaert, F. Van Laere, M. Ayre, W. Bogaerts, D. Van Thourhout, P. Bienstman, R. Baets, Jpn. J. Appl. Phys. Part 1 45 (2006) 6071.